Cell Death & Differentiation (2020) 27:2433–2450
https://doi.org/10.1038/s41418-020-0514-3

Cell Death & Differentiation

ARTICLE

The lipogenic LXR-SREBF1 signaling pathway controls cancer cell DNA repair and apoptosis and is a vulnerable point of malignant tumors for cancer therapy

Bo Yang[1,2] · Bin Zhang[3,4,5,6,7,8] · Zhifei Cao[3,4,5,6,9] · Xingdong Xu[10,11] · Zihe Huo[3,4,5,6] · Pan Zhang[3,4,5,6] · Shufen Xiang[3,4,5,6] · Zhe Zhao[3,4,5,6] · Chunping Lv[3,4,5,6] · Mei Meng[3,4,5,6] · Gaochuan Zhang[12] · Liang Dong[13] · Shucheng Shi[1,2] · Lan Yang[1,2] · Quansheng Zhou[3,4,5,6]

Received: 14 December 2018 / Revised: 23 January 2020 / Accepted: 3 February 2020 / Published online: 6 March 2020

Abstract

Cancer cells are defective in DNA repair, so they experience increased DNA strand breaks, genome instability, gene mutagenesis, and tumorigenicity; however, multiple classic DNA repair genes and pathways are strongly activated in malignant tumor cells to compensate for the DNA repair deficiency and gain an apoptosis resistance. The mechanisms underlying this phenomenon in cancer are unclear. We speculate that a key DNA repair gene or signaling pathway in cancer has not yet been recognized. Here, we show that the lipogenic liver X receptor (LXR)-sterol response element binding factor-1 (SREBF1) axis controls the transcription of a key DNA repair gene *polynucleotide kinase/phosphatase (PNKP)*, thereby governing cancer cell DNA repair and apoptosis. Notably, the PNKP levels were significantly reduced in 95% of human pancreatic cancer (PC) patients, particularly deep reduction for sixfold in all of the advanced-stage PC cases. PNKP is also deficient in three other types of cancer that we examined. In addition, the expression of LXRs and SREBF1 was significantly reduced in the tumor tissues from human PC patients compared with the adjacent normal tissues. The newly identified LXR-SREBF1-PNKP signaling pathway is deficient in PC, and the defect in the pathway contributes to the DNA repair deficiency in the cancer. Strikingly, further diminution of the vulnerable LXR-SREBF1-PNKP signaling pathway using a small molecule triptonide, a new LXR antagonist identified in this investigation, at a concentration of 8 nM robustly activated tumor-suppressor p53 and readily elevated cancer cell DNA strand breaks over an apoptotic threshold, and selectively induced PC cell apoptosis, resulting in almost complete elimination of tumors in xenograft mice without obvious complications. Our findings provide new insight into DNA repair and apoptosis in cancer, and offer a new platform for developing novel anticancer therapeutics.

Introduction

Intracellular DNA is frequently damaged by various endogenous and exogenous DNA damage agents, producing both DNA single- and double-strand breaks (DSBs). In normal cells, damaged DNA can be repaired over time by DNA repair machinery, thereby the amount of DSBs keeps low. However, DNA repair is defective in various malignant tumors and the levels of DSBs in cancer cells are high [1–4], this raises the rate of gene mutations and genome instability, resulting in carcinogenesis and malignant tumor progression [2, 5–8]. DNA repair is deficient in cancer, notably, the levels of DSBs in pancreatic tumor tissues are increased approximately eightfold compared with normal pancreatic tissues [9, 10]; however, multiple DNA repair genes and signaling

These authors contributed equally: Bo Yang, Bin Zhang, Zhifei Cao

Edited by T. Mak

Supplementary information The online version of this article (https://doi.org/10.1038/s41418-020-0514-3) contains supplementary material, which is available to authorized users.

✉ Zhifei Cao
hunancao@163.com

✉ Quansheng Zhou
zhouqs@suda.edu.cn

Extended author information available on the last page of the article

pathways are strongly activated in various types of malignant tumors [3, 4, 8]. The mechanisms underlying this phenomenon in cancer remain enigmatic.

The liver X receptors (LXRα/NR1H3, LXRβ/NR1H2) are nuclear receptors that act as master transcription factors to control the transcription of multiple lipogenic and tumorigenic genes that regulate lipid metabolism and tumorigenesis [11–17]. Aberrant expression of the *LXRs* and their downstream *sterol response element binding factor-1* (*SREBF1*, also known as *SREBP1* and *SREBP1c*) is associated with not only dyslipidemia, obesity and cardiovascular diseases [11, 12], but also various types of cancer [13–17]. However, the role of the lipogenic genes *LXRs and SREBF1* in DNA repair has not been reported to date.

Polynucleotide kinase/phosphatase (PNKP) is a unique bi-functional DNA strand end-processing enzyme essential for the repair of both single- and double-DSBs, and is required for DNA repair and the survival of cells and mammals [18–22]. Convincingly, either the knockout of *PNKP* or inhibition of PNKP enzyme activity in cancer cells causes the cells prone to apoptosis and sensitizes the cells to radiation and DNA damage drugs, resulting in synthetic lethality [23–27]. Despite the importance of PNKP, the transcription-regulatory mechanism of the gene is enigmatic, neither its function in the pancreas nor its role in pancreatic cancer (PC) have been reported in the literature.

We guess that a key DNA repair gene or signaling pathway in cancer has not yet been recognized and conducted this study to explore the mechanisms of DNA repair deficiency and apoptotic resistance in malignant tumors, focusing on PC. We found that the lipogenic LXR-SREBF1 signaling pathway controls the transcription of PNKP, thereby governing PC cell DNA repair and apoptosis, and the LXR-SREBF1-PNKP signaling pathway is a vulnerable point of malignant tumors for cancer therapy.

Results

PNKP controls cancer cell apoptosis by the regulation of DNA repair

We first screened the expression levels of DNA repair essential genes in normal cells and PC cells, and observed that PNKP expression levels were significantly reduced in six human PC cell lines compared with various normal tissues and cell lines (Fig. S1a), then we investigated whether *PNKP* is abnormally expressed in PC patients and found that the levels of PNKP protein were reduced on average 3.2-fold in tumor tissues from 124 human pancreatic ductal adenocarcinoma patients compared with matched tumor-adjacent normal tissues using the immunohistochemical staining method (Fig. 1a, b). The decrease in PNKP protein was particularly apparent in all of the advanced-stage PC patients who showed an average sixfold reduction in the protein compared with matched tumor-adjacent normal tissues (Fig. 1c); PNKP levels were also significantly lower in advanced stage (III and IV) than in early stage (I and II) PC cases (Fig. 1c). In addition, quantitative real-time PCR (qPCR) showed that *PNKP* expression levels were markedly reduced in the primary tumor tissues from 22 cases of PC patients compared with matched tumor-adjacent normal tissues (Fig. 1d). Consistent with our findings, database mining (https://www.oncomine.org) of human gene expression data showed that *PNKP* expression in pancreatic tissue samples was significantly decreased in the patients with pancreatic intraepithelial neoplasia, and was profoundly reduced in pancreatic tumor tissues compared with normal tissue (Fig. 1e). In short, these data imply that the low levels of PNKP were related to the advanced stage of the cancer.

Strikingly, PNKP levels were significantly reduced in 95% of PC cases (Fig. 1c); this is the highest defective rate among all of the 39 DNA repair genes in the cancer reported in the literature [26]. Thus, our findings show that PNKP is a useful new biomarker for PC with high sensitivity, and provide a foundation for the mechanistic study of DNA repair deficiency in the cancer. This research is particularly important for the patients with advanced-stage PC who account for > 80% of the cancer patients and for which there are no effective therapies. PNKP levels were also significantly lower in cancer cell lines derived from human PC, cervical cancer, leukemia, and lymphoma compared with immortalized normal cell lines (Fig. 1f, see also Fig. S1a, b). Database mining (https://www.oncomine.org) indicated that *PNKP* expression was also significantly decreased in the malignant tumor tissues from human cervical cancer (Fig. 1g), acute myeloid leukemia (Fig. 1h), and follicular lymphoma (Fig. 1i). Collectively, these data suggest that PNKP should be viewed as an important new biomarker for PC and three other types of malignant tumors.

Next, we investigated the role of PNKP in PC cell DNA repair and apoptosis. Silencing of PNKP by shRNA markedly increased intracellular DSBs by 167-fold in PC cells in the absence of DNA damage inducer (Fig. 2a, b, see also Fig. S1c, d for PNKP protein levels). In addition, when the cancer cells were treated with a very low dose (1 mJ/cm^2) of ultraviolet B (UVB) radiation, the level of DSBs obviously increased; furthermore, silencing of PNKP resulted in a sixfold further increase in the levels of DSBs in the cells compared with UVB radiation only (Fig. 2c, d), moreover, the PNKP-silenced cancer cells readily went to apoptosis (Fig. 2e). These data suggest that reduction of intracellular PNKP levels markedly impairs DNA repair and sensitizes PC cells to UVB

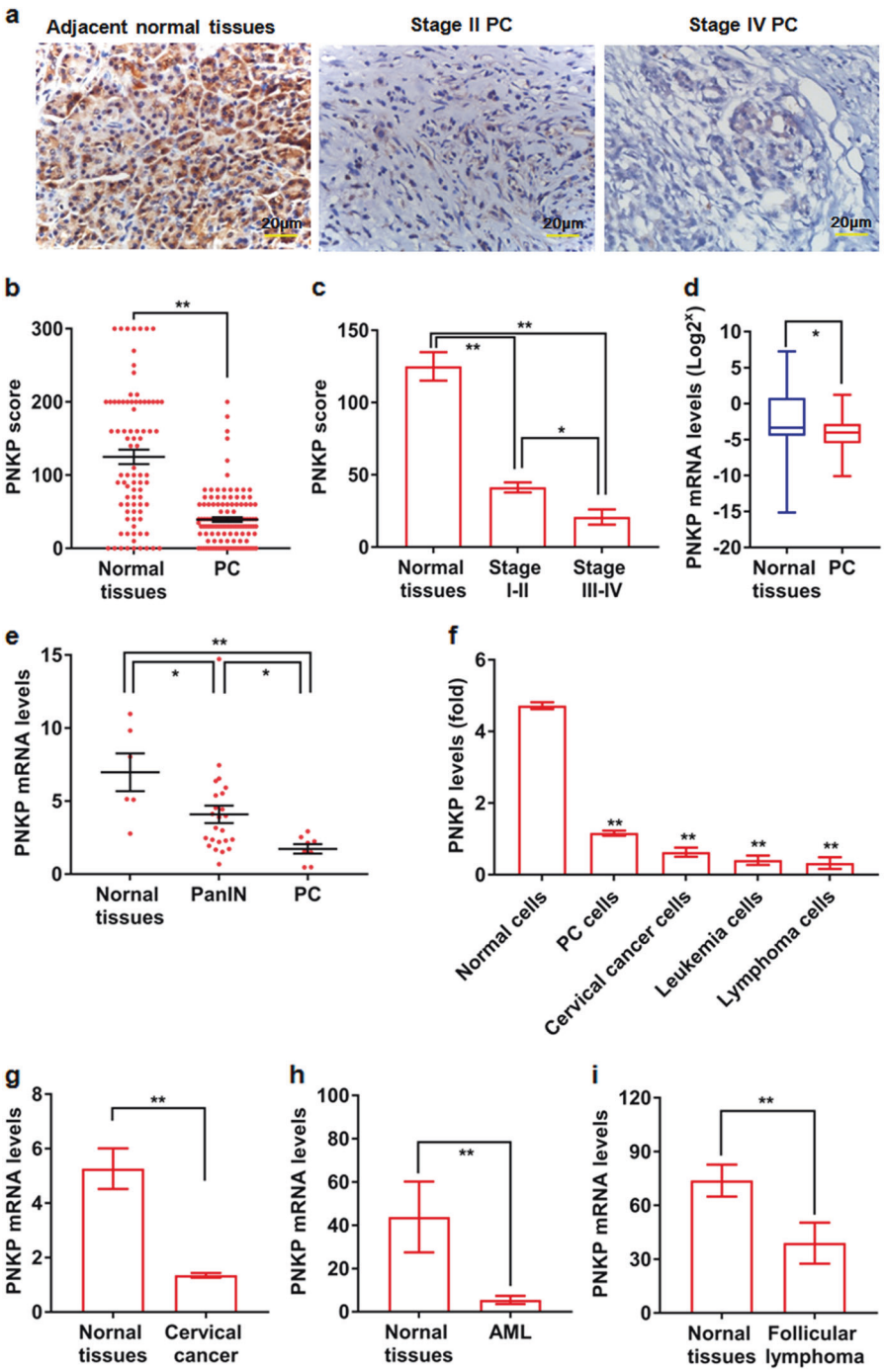

Fig. 1 PNKP is deficient in tumors from the patients suffered from pancreatic cancer and other three types of malignant tumors. Polynucleotide kinase/phosphatase (PNKP) protein in tumor tissues and matched adjacent normal tissues from 124 human pancreatic ductal adenocarcinoma (PDA) patients at the early (I–II) and advanced (III-IV) stages was detected with immunohistochemical (IHC) staining **a** and analyzed **b**, **c**. Results indicated that PNKP is deficient in pancreatic cancer (PC) tumor tissues in 95% of PC cases **b**, with a particularly severe deficiency in all of the advanced-stage PC patients (III and IV) **c**. In addition, PNKP mRNA levels in the tumor tissues and adjacent normal tissues from 22 cases of pancreatic cancer patients **d** and in the samples from four immortalized normal cell lines, six PC cell lines, three cervical cancer cell lines, three leukemia cell lines, and three lymphoma cell lines **f** were measured by qPCR. Data are shown in 1f as means ± S.E of three independent replicates. In addition, the data on PNKP mRNA levels in the patients suffering from pancreatic intraepithelial neoplasia (PanIN) and pancreatic cancer (PC) **e**, cervical cancer **g**, acute myeloid leukemia (AML, **h**), and follicular lymphoma **i**, were detected by DNA microarray, were retrieved from the publicly available cancer database Oncomine (https://www.oncomine.org), and statistically analyzed. The data are shown as mean ± S.E., the p value was determined by Student's t test. Scale bar, 200 μm.

radiation, and promotes cancer cell apoptosis. In contrast, overexpression of PNKP (Fig. S1e, f) notably diminished the levels of UVB-induced DSBs in pancreatic cell lines (Fig. 2f, g) and the pancreatic tumor cells from tumor-bearing xenograft mice (Fig. S2a–d), and reduced cancer cell apoptosis (Fig. 2h). Furthermore, inhibition of PNKP activity via its specific inhibitor A12B4C3 [23, 24] significantly induced apoptosis in PC cell lines Patu8988 (Fig. 2i, j) and Panc1 (Fig. S1g). Together, these results suggest that PNKP controls PC cell DNA repair and apoptosis.

The lipogenic LXR-SREBF1 signaling pathway controls PNKP gene transcription and functions as a new regulator of DNA repair and apoptosis in cancer

The regulatory mechanisms that control the transcription of *PNKP* remain enigmatic. The *PNKP* gene promoter region

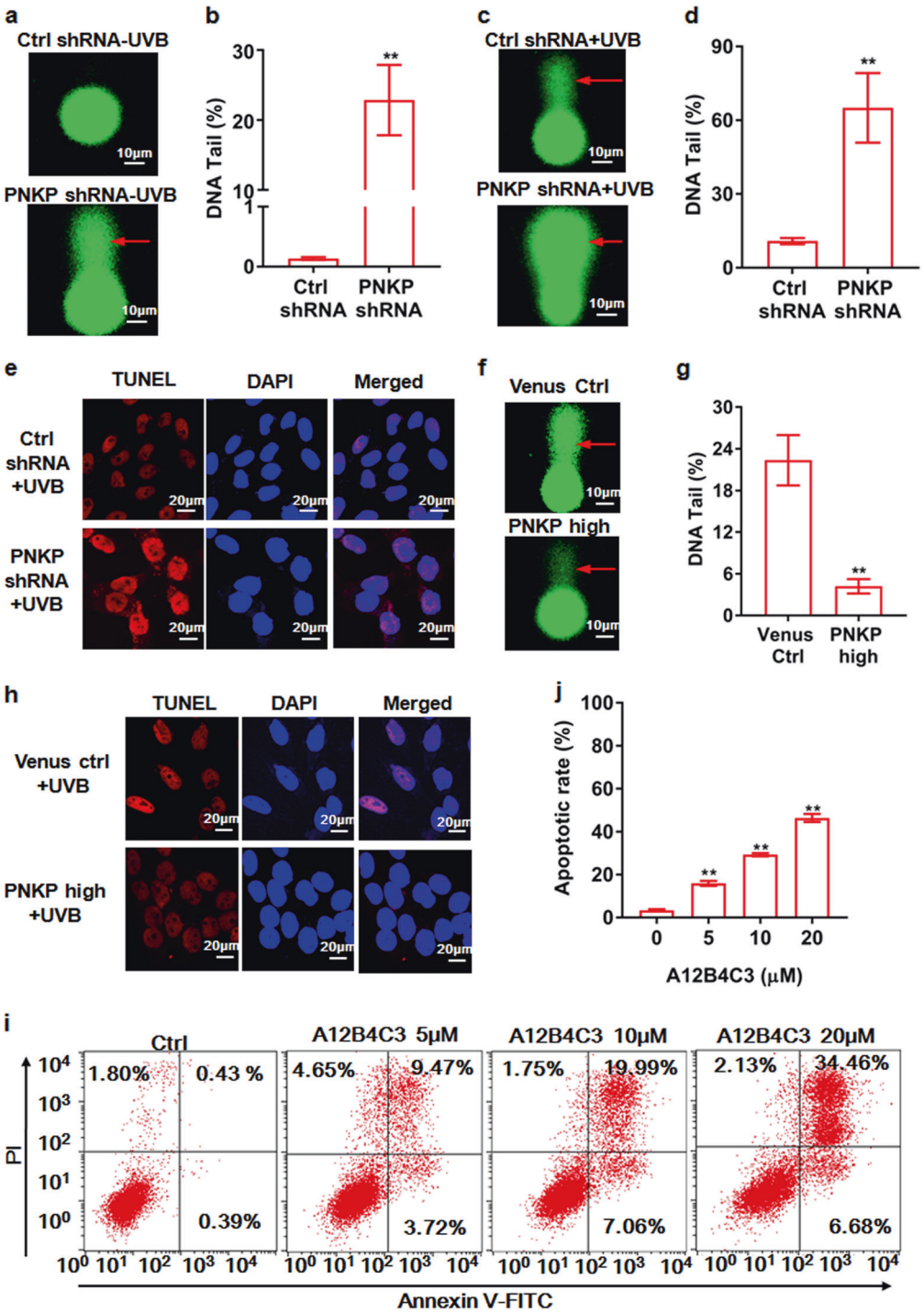

Fig. 2 PNKP controls the levels of intracellular DNA double-strand breaks and apoptosis as well as tumorigenicity of pancreatic cancer cells. Silencing of PNKP by shRNA along (see Fig. S1c, d) markedly increased DNA single- and double-strand breaks (DSBs) in pancreatic cancer (PC) cell line Patu8988 measured by a comet assay **a**, **b** and further significantly increased DSBs upon radiation of the PC cells with a very low dose (1 mJ/cm^2) ultraviolet beam (UVB) **c**, **d** as indicated by the red arrow **a** and **c**, the apoptotic cells (red) were detected by TUNEL assay **e**. In contrast, over-expression of PNKP (PNKP high, see Fig. S1e, f) diminished DSBs upon radiation with 2 mJ/cm^2 UVB **f**, **g** and reduced apoptotic cells (red) as measured by TUNEL assay **h**. Inhibition of PNKP activity using its specific inhibitor A12B4C3-induced PC cell apoptosis as measured by PI-Annexin V double staining **i**, **j**. Data are shown as means ± S.D. of three independent replicates. Scale bar, 20 μm.

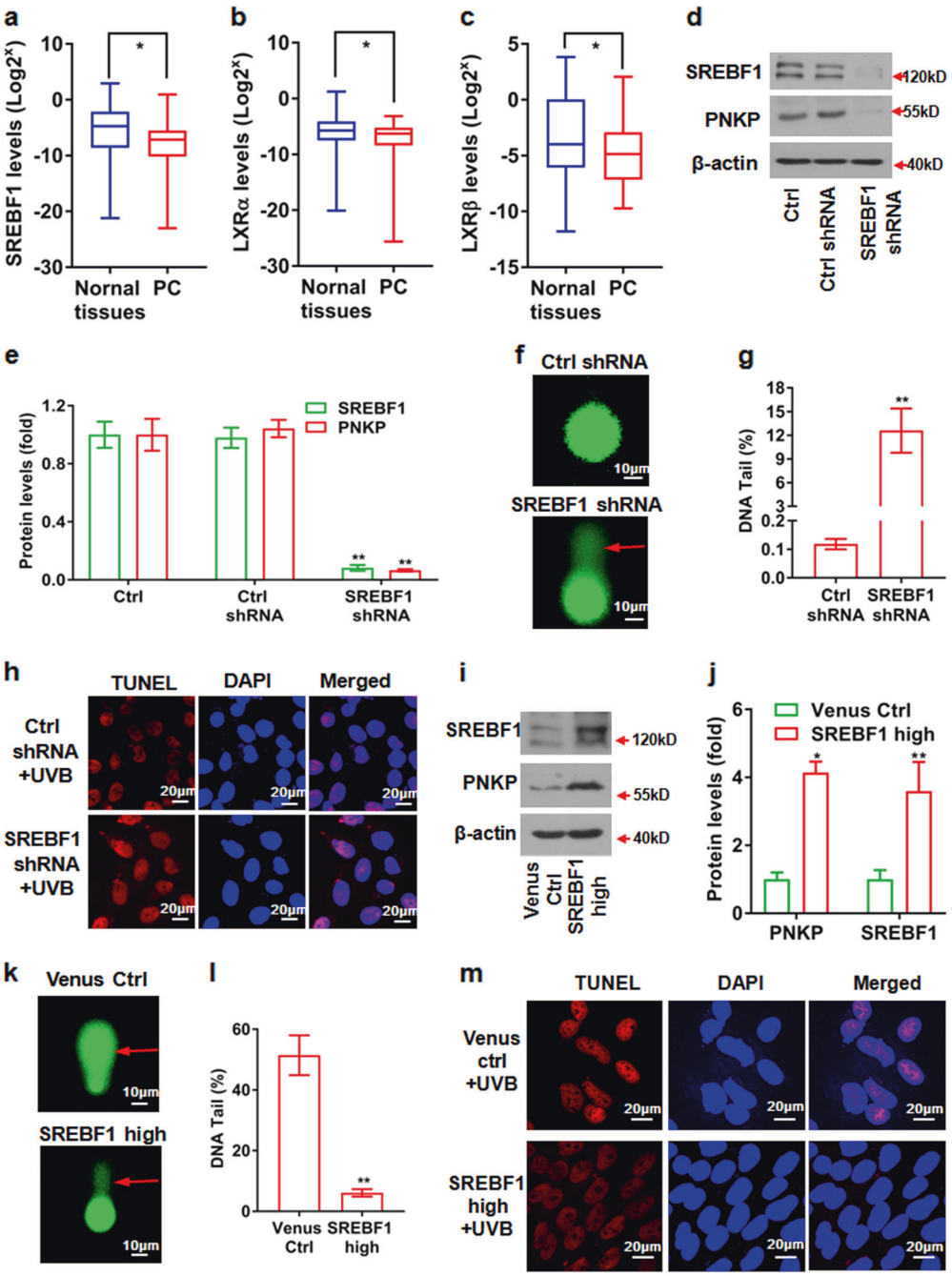

Fig. 3 SREBF1 regulates *PNKP* gene expression and governs pancreatic cancer cell DNA repair and apoptosis. The mRNA levels of *SREBF1* **a**, *LXRα* **b**, and *LXRβ* **c** in the tumor tissues and adjacent normal tissues from 22 cases of pancreatic cancer patients were measured by qPCR. Silencing of the transcription factor SREBF1 expression by shRNA significantly diminished PNKP expression levels **d**, **e**, increased DNA single- and double-strand breaks (DSBs) in pancreatic cancer (PC) cells (red arrows in **f**, **g**) and apoptotic cells (red) as detected by TUNEL assay **h**. By contrast, overexpression of SREBF1 significantly increased expression of the *PNKP* gene **i**, **j**, decreased intracellular DSBs **k**, **l** and apoptotic cells **m**. Data are shown as mean ± S.D. based on three independent replicates. Scale bar, 20 μm.

is predicted to contain a sterol response element (SRE) that may be bound by the transcription factor SREBF1 (Fig. S3a). *SREBF1* transcription is driven by LXRs [28] (Fig. S3b), so we examined the expression of *LXRα and LXRβ* in PC. qPCR analysis revealed that the expression levels of *SREBF1* (Fig. 3a), *LXRα* (Fig. 3b), *and LXRβ* (Fig. 3c) were reduced in the primary tumor tissues from 22 cases of PC patients compared with matched tumor-adjacent

normal tissues. In addition, compared with normal cells, the expression of both the *SREBF1* (Fig. S3c) and *LXRα* (Fig. S3d) genes was downregulated by approximately fourfold in all six tested PC cell lines. Consistent with our results, database mining (https://www.oncomine.org) of human gene expression data showed that the expression levels of both *SREBF1* (Fig. S3e) and *LXRα* (Fig. S3f) were significantly reduced in the tumor tissues from PC patients compared to the pancreatic tissues from normal people.

Next, we investigated whether *PNKP* expression in PC cells was controlled by SREBF1. The silencing of SREBF1 using shRNA in PC cell Patu8988 markedly reduced expression of *PNKP* (Fig. 3d, e), increased intracellular DSBs (Fig. 3f, g) and the levels of the DNA strand break marker γH2AX (Fig. S3g, h), and induced cancer cell apoptosis (Fig. 3h). Similarly, inhibition of SREBF1 activity via treatment with its specific inhibitor FGH10019 [29] suppressed *PNKP* expression in a dose-dependent manner (Fig. S3i, j), increased the number of intracellular DSBs (Fig. S3k–n). In contrast, overexpression of SREBF1 significantly increased PNKP levels in PC cells (Fig. 3i, j), but markedly reduced the levels of DSBs in the cancer cells by 8.3-fold (Fig. 3k, l) and diminished apoptosis (Fig. 3m). The similar effect of SREBF1 on DNA repair (Fig. S4a, b) and apoptosis (Fig. S4c–f) was observed in another PC cell line Panc1. These findings suggest that the transcription factor SREBF1 controls *PNKP* expression, DNA repair, and apoptosis of the cancer cells.

The transcription factor LXRα is upstream of SREBF1 [28]. Next, we investigated the impact of LXRα on the expression of the *SREBF1* and *PNKP* genes. Overexpression of LXRα notably elevated SREBF1 and PNKP protein levels in PC cells (Fig. 4a, b), but diminished UVB-induced cancer cell apoptosis (Fig. 4c). In contrast, silencing of LXRα significantly reduced SREBF1 and PNKP protein levels in PC cells (Fig. 4d, e), but increased the amount of intracellular DSBs after UVB radiation (Fig. 4f, g) and apoptosis in both PC cell lines Patu8988 (Fig. 4h) and Panc1 (Fig. S5a–d). In addition, activation of LXRα in PC cells by treatment with its specific agonist GW3965 promoted LXR downstream *SREBF1* (Fig. 4i, l) and *PNKP* expression (Fig. 4i, k). Strikingly, inhibition of LXRα activity via a very low concentration of triptonide (8 nM) almost completely suppressed transcription of *SREBF1* and *PNKP* in PC cells (Fig. 4i, k, l, see also Fig. S6a–f). Interestingly, the low concentration of triptonide also notably increased the number of DSBs in *PNKP*-deficient PC Panc1 and Patu8988 cells, but only moderately elevated the levels of DSBs in the immortalized normal Chang liver cell line with normal PNKP expression (Fig. S5h, i), suggesting that triptonide selectively promotes the genesis of DSBs in PC cells via inhibition of the LXRα downstream *SREBF1* and *PNKP* gene transcription. Taken together, these findings suggest that DNA repair in PC cells is controlled by the newly identified LXRα-SREBF1-PNKP signaling pathway.

A new anticancer strategy for creating a bottleneck to selectively reduce DNA repair and apoptotic resistance in cancer cells

Next, we explored a new strategy for developing novel cancer therapy. Noticeably, the LXR-SREBF1-PNKP signaling pathway can be almost completely inhibited by 8 nM triptonide, a small molecule with anticancer effect [30–34], but the effect of triptonide on DNA repair has not yet been reported. A mechanistic study showed that triptonide did not affect the expression of the *LXRβ* and *LXRβ* genes (Fig. S5e), but strongly suppressed transcription of downstream *SREBF1* and *PNKP* genes (Fig. 4i–l, see also Fig. S6a–f). These results suggest that LXR is the first protein in the LXR-SREBF1-PNKP signaling axis. It is well established that sterols bind to their receptor proteins LXRα and LXRβ, activating the proteins, which function as transcription factors to drive the expression of various lipogenic and oncogenic genes [11–17]. Triptonide has a similar backbone chemical structure with sterols. Accordingly, we hypothesized that triptonide might bind to the proteins of LXRs and inhibit the LXR-SREBF1-PNKP signaling pathway.

The binding of triptonide to LXRs has not yet been reported in the literature, therefore, we studied the direct binding of triptonide to LXR proteins using three independent methods, focusing on LXRα, because LXRα is expressed in various tissues, including liver, adrenal gland, intestine, adipose tissue, macrophages, lung, kidney, and pancreas, whereas LXRβ is ubiquitously expressed in a few of tissues. Surface plasmon resonance (SPR) analysis indicated that triptonide binds directly to LXRα, with extremely high affinity constants of 0.12 nM and 43.2 nM, respectively, for the fast and slow binding phases (Fig. 5a, b). This direct interaction was further confirmed by pull-down assay, high-performance liquid chromatography (HPLC), and mass spectrometry (Fig. 5c, d). In addition, circular dichroism (CD) analysis showed that triptonide caused the second structure changes in LXRα protein (Fig. 5e). Collectively, these results imply that LXRα functions as a very high affinity receptor for triptonide.

In addition, we found that triptonide potently inhibited proliferation of all six of the human PC cell lines that we tested, with an average IC_{50} of 10.3 ± 2.8 nM, particularly, the IC50 was 7.8 nM and 9.7 nM for the highly malignant PC cell lines Patu8988 and Panc1, respectively (Fig. 6a). Treatment with 8 nM triptonide remarkably inhibited LXRα function and expression of downstream *PNKP* and *SREBF1* genes and notably induced accumulation of DSBs in PC cells as

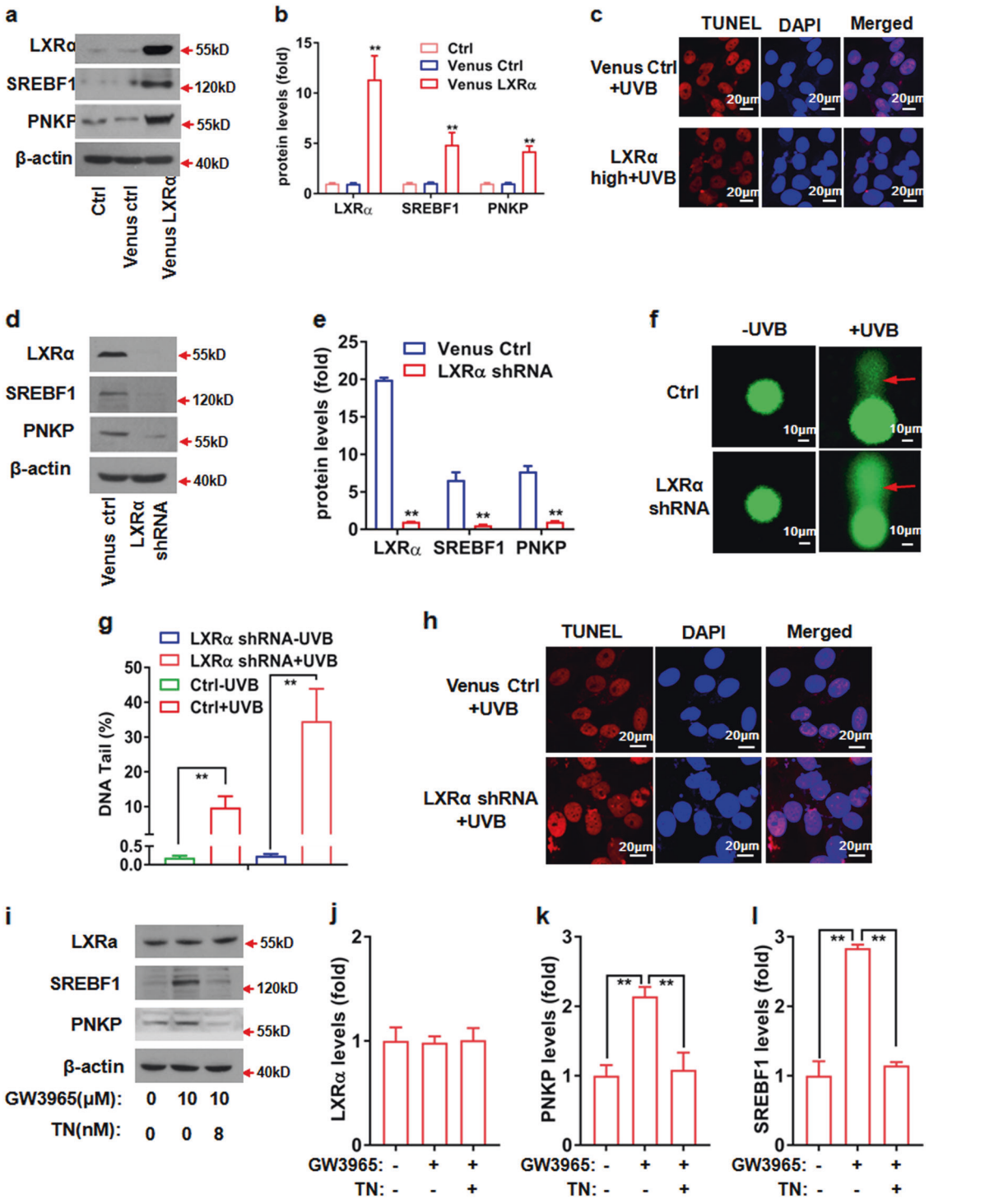

Fig. 4 The LXRα controls pancreatic cancer cell DNA repair and apoptosis by the regulation of downstream SREBF1 and PNKP expression. Overexpression of LXRα (LXRα high) significantly increased expression of the SREBF1 and PNKP in pancreatic cancer cells **a**, **b**, but reduced apoptotic cells (red) as detected by TUNEL assay **c**; In contrast, silencing LXRα (LXRα shRNA) resulted in reduction of SREBF1 and PNKP expression levels **d**, **e**, but significantly increased the levels of DNA single- and double-strand breaks (DSBs, red arrows, **f**, **g**) and apoptotic cells **h**. Activation of LXRα and/or LXRβ by its specific agonist GW3965 promoted SREBF1 and PNKP expression in pancreatic cancer cells (**i** middle lane, **k**, **l**). Strikingly, GW3965-induced expression of SREBF1 and PNKP was almost completely abolished by triptonide (TN) in pancreatic cancer Patu8988 cells (**i** right lane, **k**, **l**), whereas the levels of LXRα were not significantly affected (**i** right lane, **j**), similar results were observed at mRNA levels in pancreatic cancer Panc1 cells (Figs. S3, S4). Scale bar, 20 μm. The complete western blotting gels in Fig. 4 are presented in Fig. S10.

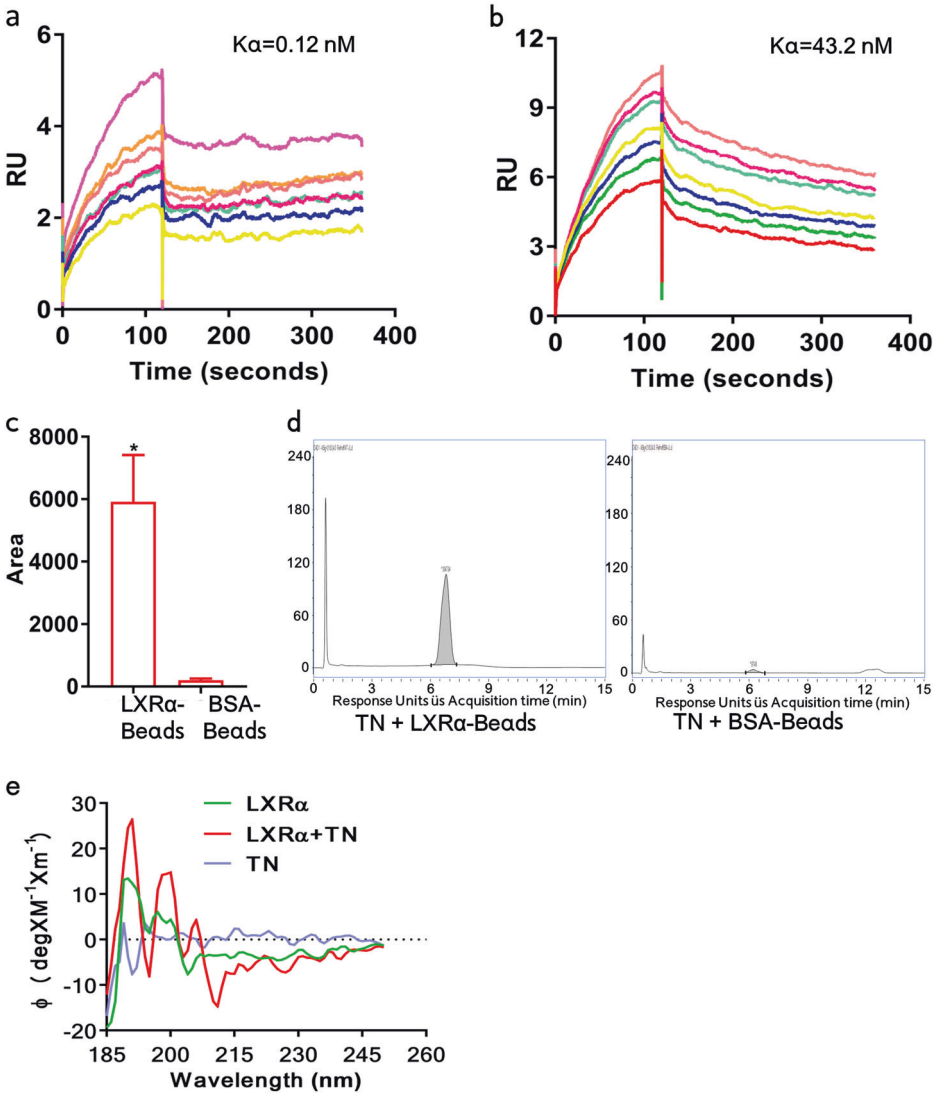

Fig. 5 Triptonide directly binds to its receptor LXRα with extreme high affinity. The direct binding between triptonide (TN) and LXRα was ascertained by the surface plasmon resonance (SPR) assay and displayed extremely high affinity constants (*Kd*) of 0.12 nM **a** and 43.2 nM **b**, for the fast and slow binding phases, respectively. The binding of triptonide to LXRα was further confirmed by pull-down assay, followed by high-performance liquid chromatography (HPLC) and mass spectrometry **c**, **d**, and circular dichroism (CD) analysis **e**. Apparently, much more TN bound to the LXRα-beads than the control BSA-beads **c**, and HPLC showed a high pick in the group of TN + LXRα-beads **d**, and CD analysis indicated three distinct high peaks and low peak after incubation of LXRα with TN **e**.

mentioned above. Triptonide caused enlargement of PC cell size, in particular, an enlarged nucleus was apparent in the cancer cells, leading to the formation of large cells with two or more micronuclei, leading to the formation of large nonviable cells with two or more micronuclei (Fig. 6b–d). Our cell cycle analysis indicated that the PC cell cycle was arrested at the G2/M phase after triptonide treatment [34]. These results suggest that triptonide promotes tumor cell mitotic catastrophe. Consequently, PC cells became apoptotic after treatment of Patu8988 (Fig. 6e, f) and Panc1 (Fig. 6g, h) cell lines with 8 nM triptonide for 9 days (Fig. 6e–h). Triptonide induces PC cell apoptosis in a time-dependent manner (Fig. S7g, h). Furthermore, compared with PNKP and LXRα low expression cells, overexpression of PNKP (Fig. S7a, c) and LXRα (Fig. S7b, d) in PC cell line Patu8988 reduced the amount of apoptotic cells (Fig. S7b, d), but increased cancer cell survival (Fig. S7e, f), suggesting that PNKP and LXRα play a role in the regulation of PC cell apoptosis.

More interestingly, suppression of the LXRα-SREBF1-PNKP axis by 8 nM triptonide markedly elevated the levels of both phosphorylated p53 (43.5-fold increase) and total p53 (4.2-fold increase; Fig. 7a–c), moreover, 8 nM triptonide treatment significantly suppressed the colony-forming capabilities of PC cells (Fig. 7d, e), suggesting that triptonide is a new p53 activator and cancer cell apoptosis inducer.

Finally, we evaluated the antitumor efficacy of the newly identified LXR antagonist triptonide in human PC cell Patu8988 xenograft mouse model. Strikingly, in the tumor treatment model, the tumors in five of eight xenograft mice were completely eliminated after administration of 5 mg/kg/d triptonide for 73 days (Fig. 7f, g), and the tumor volumes of the remaining three mice were markedly reduced; the overall inhibition rate was 99.6% (Fig. 7h). Of note, there were no significant differences in the body weight, organ index, or blood cell parameters between the triptonide-treated and control mice (Fig. S8a–e), suggesting that triptonide does not cause

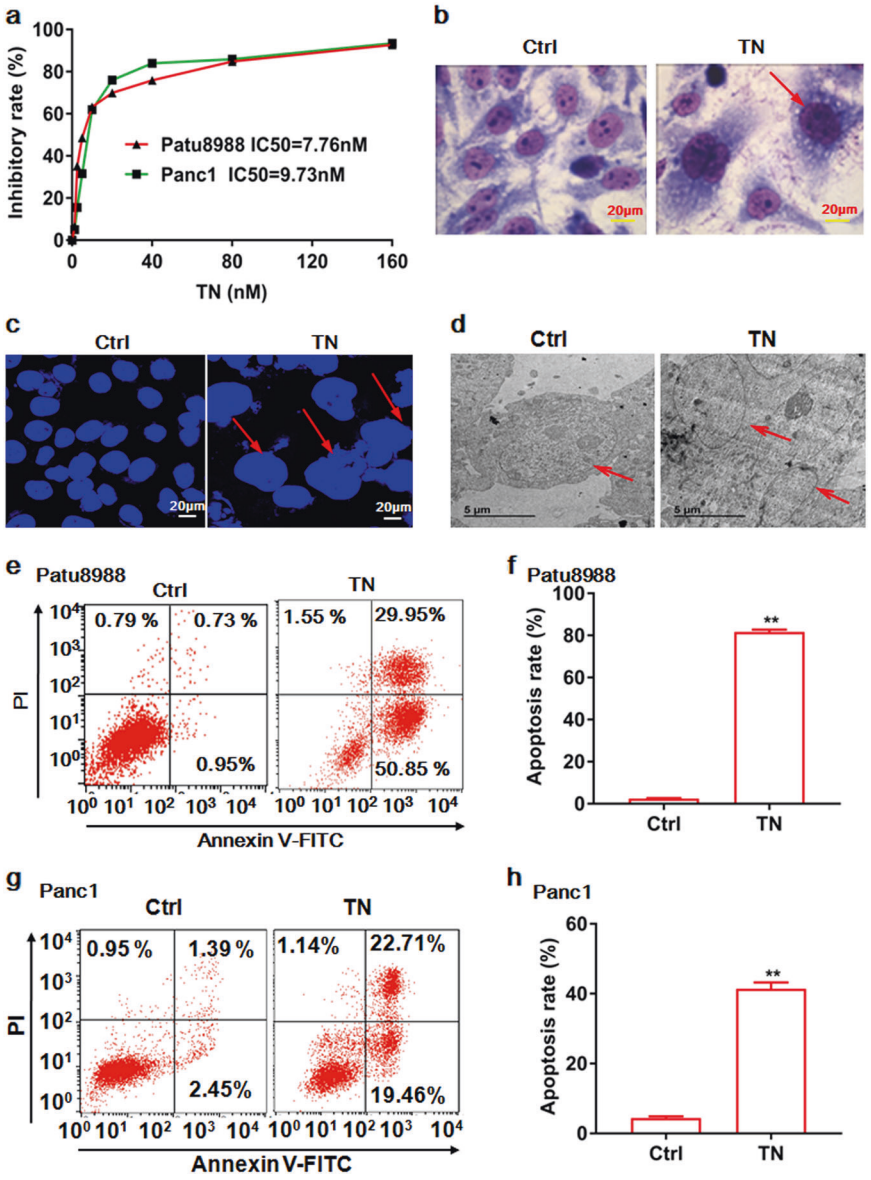

Fig. 6 Triptonide promotes tumor cell mitotic catastrophe and apoptosis. Triptonide (TN) strongly inhibited pancreatic cancer cell growth with an extremely low IC_{50} of 7.76 nM for pancreatic cancer cell line Patu8988, and 9.73 nM for Panc1 **a**, respectively, and caused enlargement of the cell nuclei (red arrows) as shown by Giemsa–Wright staining (**b**, scale bar, 50 μm), DAPI staining (**c**, scale bar, 20 μm), and electronic microscope imaging (**d**, scale bar, 5 μm). After treatment of pancreatic cancer Patu8988 (**e**, **f**) and Panc1 (**g**, **h**) cell lines with 8 nM TN for 9 days, the cells succumbed to apoptosis (red) as detected by and Annexin V double staining and flow cytometry. Data are shown as mean ± S.E. of three independent replicates.

severe complications at the effective anti-PC doses tested. Together, these results indicate that targeting the LXR-SREBF1-PNKP axis using triptonide effectively suppresses PC cell DNA repair, induces cancer cell apoptosis, and inhibits tumor growth, offering a potential new strategy to treat PC (Fig. 8).

Discussion

The LXR-SREBF1 signaling pathway acts as a new regulator in DNA repair and apoptosis in cancer

DNA repair is known to be defective in various cancers [1–4, 26], yet many well-known classic DNA repair genes and pathways are robustly activated in various cancers, including PC [2, 3, 8–10]. The contradiction between DNA repair deficiency and strong activation of multiple, classic DNA repair genes, and pathways in cancer has puzzled cancer researchers for several decades. In the current study, we uncover that the lipogenic LXR-SREBF1-signaling pathway controls the transcription of key DNA repair gene *PNKP*, thereby governing cancer cell DNA repair, apoptosis, and tumorigenicity. Our findings provide new insight into DNA repair and apoptosis in cancer.

Furthermore, inhibition of the LXRα-SREBF1-PNKP signaling pathway by triptonide creates a controllable bottleneck boosting intracellular DSBs over the apoptotic threshold in cancer cells, and readily induces cancer cell apoptosis. Our findings provide new strategy for controlling DNA repair and apoptosis in cancer.

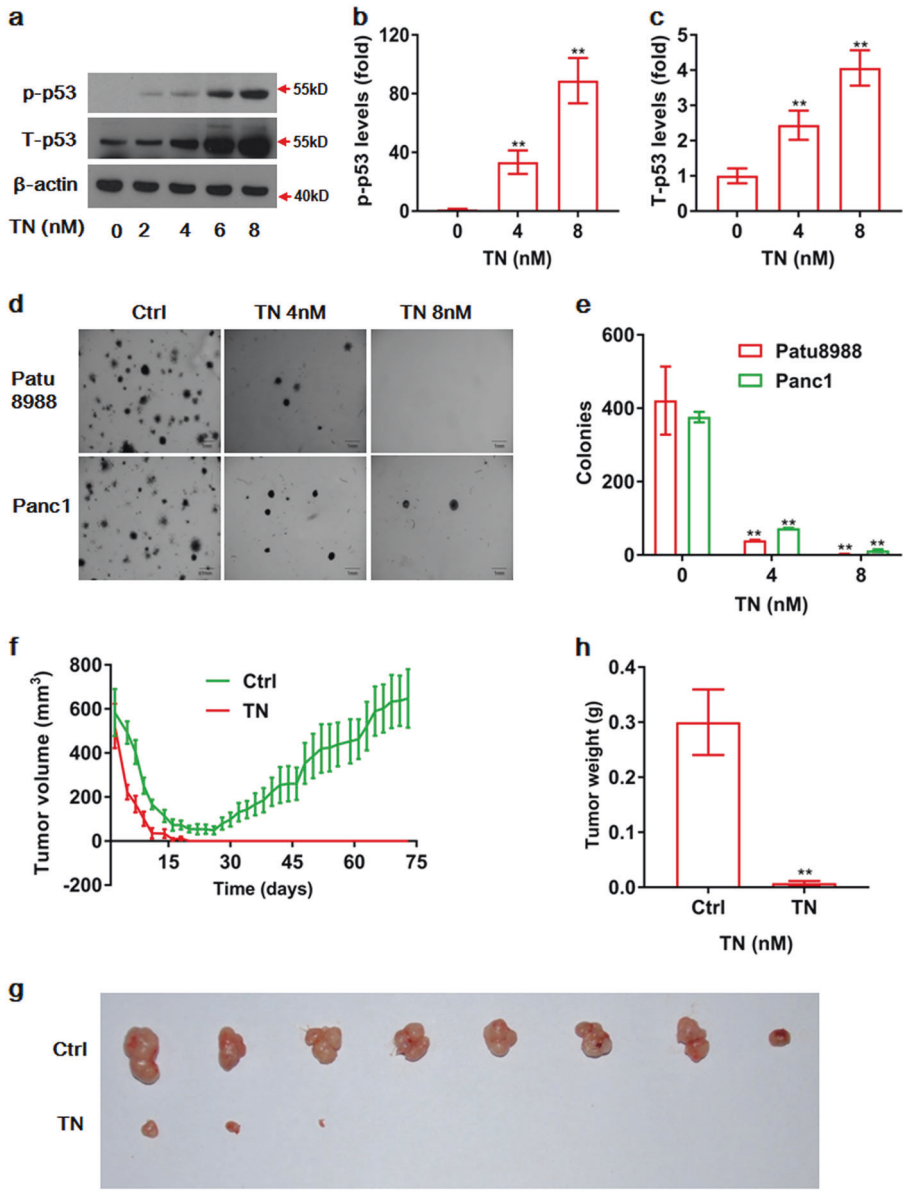

Fig. 7 Triptonide strongly activates p53 and markedly suppresses pancreatic cancer cell tumorigenicity and tumor growth in vivo and significantly prolongs the survival of tumor-bearing xenograft mice. Triptonide (TN) at 8 nM markedly increased the protein levels of phosphorylated tumor-suppressor p53 (p-p53) **a**, **b** and also significantly promoted expression of total p53 protein (T-p53) in pancreatic cancer (PC) cells **a**, **c**. PC cell colony-forming capability was inhibited by treatment with 8 nM TN (**d**, quantitation in **e**). The anti-PC efficacy of TN was evaluated in a mouse model. Of note, human pancreatic cancer Patu8988 cells and Matrigel were first incubated at 4 °C for 10 min and mixed, and then subcutaneously injected 300 µl of the mixture to the back each mouse. The cold Matrigel is a liquid, but it becomes solid at 37 °C in mice. The tumor volume was monitored using digital calipers every other day **f**, the initial tumor volume reflects the mixture of injected Matrigel and tumor cells. The Matrigel was gradually degraded in the xenograft mice within 2 weeks after injection, thereby gradually decreasing the tumor volume during the initial 2 weeks **f**. The tumors in five of eight xenograft mice were completely eliminated after TN treatment for 73 days at 5 mg/kg/d, and tumors in the remaining three mice were markedly reduced (**g**, quantitation in **h**). Data in 7a–e are shown as means ± S.E. of three independent replicates.

A new platform to develop LXR antagonists and novel anticancer therapeutics

LXRs play a divergent role in tumorigenesis, functioning as either tumor-suppressor [35–38] or tumor-promoter dependent on the cell types and animal species [39–48]. The tumor-suppressive effect of LXRs has been extensively studied in recent decades, and activation of LXRs has been generally applied as a strategy for cancer therapy [35–52]. Several LXR agonists, such as T0901317, GW3965, and LXR-623, exhibit anti-atherosclerosis, anti-inflammation, and anticancer effects in mouse models [49–51], and have

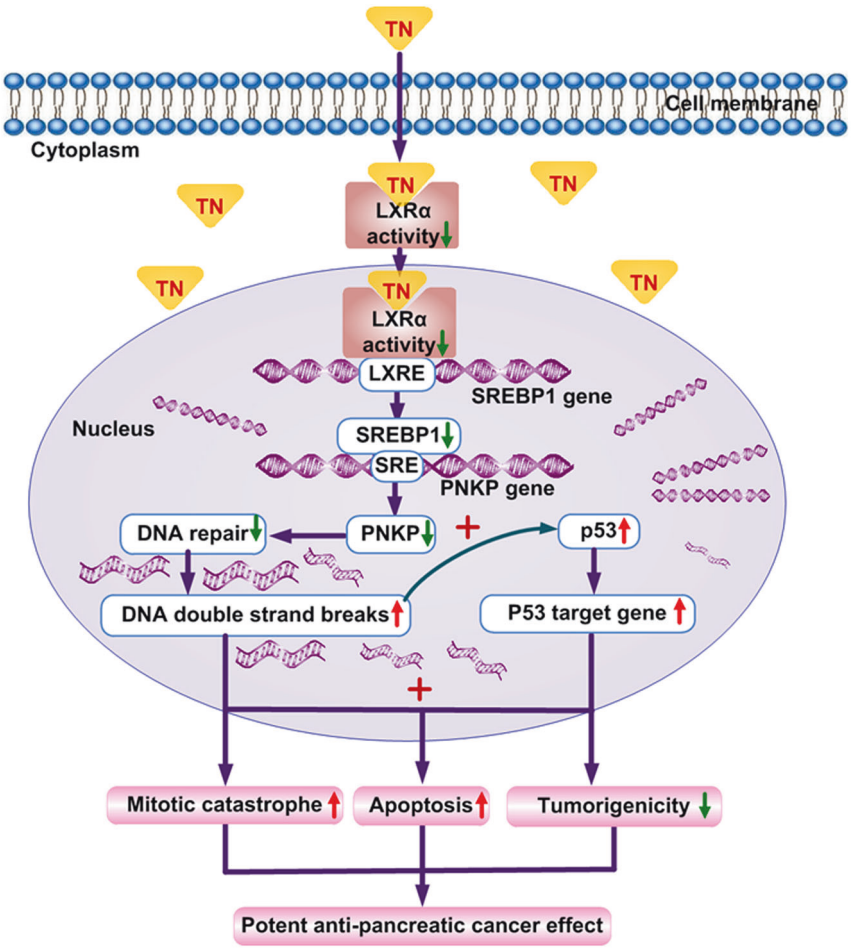

Fig. 8 Schematic diagram showing that the LXRs-SREBF1-PNKP axis is essential for DNA repair in cancer cells and is a vulnerable point of pancreatic cancer for effective cancer therapy. Hydrophobic triptonide (TN) passes through the cell membrane and directly binds to its receptor liver X receptors (LXRα and/or LXRβ), inhibits the transcriptional activity of LXRs and reduces the expression of LXR downstream transcription factor *SREBF1* gene, in turn diminishing SREBF1-downstream *PNKP* gene expression. The LXRs-SREBF1-PNKP signaling axis controls the levels of intracellular DNA single- and double-strand breaks (DSBs) and DNA repair in pancreatic cancer (PC) cells. Reduction of the LXRs-SREBF1-PNKP axis by triptonide causes a severe defect in DNA repair, marked elevation of intracellular DSBs, activation of p53, and induction of PC cell mitotic catastrophe and apoptosis, resulting in marked reduction of PC cell tumorigenicity and potent anti-PC effects without obvious complications in murine studies.

been evaluated in five early clinical trials (four phase I and one phase 2a) [12, 35, 50–52], unfortunately, none have progressed to further clinical trial so far because of multiple adverse reactions such as hypertriglyceridemia, liver steatosis, neurological, and psychiatric events [52]. Of note, the tumorigenic function of LXRs has not yet received due attention.

Emerging evidence shows that LXRα is overexpressed in gastric cancer tumor tissues and increases cancer cell motility and invasion capabilities; in contrast, silencing LXRα expression inhibits cancer cell migratory capability [14]. Overexpression of LXRα/LXRβ is closely associated with poor overall survival in the cancer patients [39]. In addition, activation of LXRα and LXRβ by cholesterol in malignant ascites promotes chemoresistance in ovarian cancer, contributing to poor prognosis in ovarian cancer patients [40]. Furthermore, LXRα promotes renal cancer cell metastasis by regulating the NLRP3 inflammasome in renal cell carcinoma [41]. Moreover, cholesterol and 27-hydroxycholesterol activate LXRs and estrogen receptors to promote tumorigenesis and cancer metastasis [39–45, 53–55]. Besides, aberrant overexpression of SREBF1 promotes tumorigenesis [13–17]. Cholesterol-induced overexpression of *PNKP* and several other genes enhances leukemia cell proliferation and aggressiveness [56]. Thus, either overexpression or aberrant activation of LXRs and downstream SREBFs and PNKP promotes development of cancer, which is associated with cancer metastasis and the poor prognosis of cancer patients [13–17, 39–45, 53–55, 57]. In this study, we demonstrated that overexpression of LXRα,

SREBF1, and PNKP in PC cells promoted the apoptosis resistance of the cells; in contrast, silencing of the expression of these genes diminished cancer cell apoptosis resistance, highlighting that inhibition of the LXR-SREBF1-PNKP axis is a reasonable strategy for cancer therapy.

The serviceability of LXR antagonist in cancer therapy has not been reported to date in the literature. In this study, we find that the LXRα antagonist triptonide effectively inhibits DNA repair in cancer and selectively triggers cancer cell apoptosis, resulting in high anticancer efficacy. Amazingly, triptonide has extreme high affinity with LXRα ($Kd = 0.12$ nM) and effectively inhibits the LXRα-SREBF1-PNKP axis, cancer cell DNA repair, and tumorigenicity. Our findings support the notion that LXR antagonist is potential new anticancer therapeutics, and provide a new platform for developing novel anticancer therapeutics.

Traditionally, the overexpressed oncogenes and strongly activated tumorigenic signal pathways have been targeted for cancer therapy. Out of the ordinary, we target the vulnerable spot LXRα-SREBF1-PNKP axis of PC using LXR antagonist for cancer therapy. Our rationale is based on that the levels of DSBs are much higher in malignant tumors and are already in close proximity to the apoptotic threshold in malignant tumors [3, 4, 9, 10], therefore, a small reduction of the LXRα-SREBF1-PNKP signaling activity by triptonide readily boosts intracellular DSBs over the apoptotic threshold and induces PC cell apoptosis (Fig. S9a, b). As normal cells have high levels of PNKP, strong DNA repair capability, and fewer DSBs, treatment of the cancer cells with 8 nM triptonide only moderately raises the levels of DSBs, which do not exceed the apoptotic threshold and induce apoptosis (Fig. S9b). Our findings provide a new platform to develop novel therapeutics against cancer and offer an alternative strategy for effective cancer therapy.

Broad significance of targeting the LXRα-SREBF1-PNKP axis for anticancer therapies

In the LXRα-SREBF1-PNKP axis, each gene is necessary for DNA repair and each gene can be targeted independently, thus broadening the avenue for DNA repair- and apoptosis-based novel anticancer drug discovery. Aberrant expression or activation of LXRα and SREBF1 are associated with dyslipidemia and obesity, which are major risk factors associated with development of cancer [13–17]. Because of this, targeting the LXRα-SREBF1-PNKP axis likely exerts a twofold anticancer effect: on one hand, it suppresses the oncogenic 27-hydroxycholesterol-induced carcinogenesis [42–45, 48, 53–55, 58], and on the other hand it inhibits DNA repair and induces cancer cell apoptosis. Therefore, our approach actually represents a twofold antitumor strategy, potentially resulting in effective anticancer treatments.

In addition, the combination of the LXRα-SREBF1-PNKP axis inhibitors, like triptonide, with existing genotoxic drugs or radiation can likely yield synergistic effects for killing cancer cells [34, 59–63], thereby potentially decreasing the required doses of chemotherapy and/or radiotherapy and resulting in high anticancer efficacy with minimal complications.

Furthermore, our data show that PNKP is deficient in not only PC, but also cervical cancer, acute myeloid leukemia, and follicular lymphoma, and the deficiency of PNKP contributes to the elevation of DSBs in PC cells and render the cells prone to apoptosis. No wonder, further diminution of the vulnerable LXR-SREBF1-PNKP signaling pathway using triptonide readily increases the levels of DSBs above an apoptotic threshold and causes cancer cell apoptosis, resulting in potent anti-leukemia, anti-lymphoma, and anti-angiogenesis effects [31–33], as well as a strong anti-PC effect; hence, LXRs, SREBF1, and PNKP are potential targets for the development of novel therapies against various malignant tumors with defects in the LXR-SREBF1-PNKP signaling pathway and *PNKP* expression. Therefore, our findings have significance for cancer therapies more broadly.

Materials and methods

Materials

Triptonide was purchased from Chengdu Must Biotech Ltd (Chengdu, China). AlamarBlue Assay kit was obtained from Invitrogen (Carlsbad, CA, USA). TaqDNA polymerase was from TaKaRa Biotechnology Co., Ltd (Dalian, China). RevertAid First-Strand cDNA Synthesis Kit was obtained from Fermentas Life Sciences (St. Leon-Rot, Germany). The human normal tissue cDNA library was purchased from TaKaRa Biotechnology Co., Ltd. The PNKP inhibitor A12B3C4 (#1005129-80-5), insulin, and monoclonal antibody against β-actin were obtained from Sigma (St. Louis, MO, USA). Comet assay reagents were purchased from Trevigen (Gaithersburg, MD, USA). TUNEL assay kit was purchased from Millipore (Bedford, MD, USA). The SREBF1 inhibitor FGH10019 (#1046045-617, Lot: HY-16207) was purchased from Selleck (Houston, TX, USA). LXR agonist GW3965 (#405911-17-3, Lot31561) and LXR antagonist GSK2033 (1221277-90-2, Lot28434) were purchased from MedChem Express (Monmouth Junction, New Jersey, USA). Antibodies to PNKP (Ab181107, Lot: GR164529-2), SREBF1 (Ab135133), and LXRα (Ab176323, Lot: GR139087-7) were obtained from Abcam Ltd (Cambridge, MA, USA).

The primers for RT-PCR and qPCR were synthesized in Genwiz (Suzhou, China) and listed as following:

Gene name	Primer name	Primers sequences (5′–3′)	Assay
β-actin	Forw	AAGAGCTACGAGCTGCCTGACG	RT-PCR
	Rev	CGCCTAGAAGCATTTGCGGTGG	
PNKP	Forw	GGCCTGTTACCATCCATCCC	RT-PCR
	Rev	TGGGACTTCCGGAGCAGTTA	
SREBF1	Forw	CATCCAAACACAACCTTATTTGCAC	RT-PCR
	Rev	CACTGGATGAGTGAATGAATGTGAG	
LXRα	Forw	GAGTGAGAGTATCACCTTCCTCAAG	RT-PCR
	Rev	GATCTTCAGACACAGCACAGTGTTA	
LXRβ	Forw	GTATTTGAGTAGCGGCGGTGTG	RT-PCR
	Rev	CGCTCTGGTTCCTCTTCGGGAT	
β-actin	Forw	CACCATTGGCAATGAGCGGTTCC	qRT-PCR
	Rev	GTAGTTTCGTGGATGCCACAGG	
PNKP	Forw	TCTGGTGTCCCAAGATGAGA	qRT-PCR
	Rev	CTGCGGTGAACACTAGCAAC	
SREBF1	Forw	GAGCGAGCACTGAACTGTGT	qRT-PCR
	Rev	GGAGAAGCTGTAGGCAGGAG	
LXRα	Forw	CCCCTTCAGAACCCACAG	qRT-PCR
	Rev	TCGCAGCTCAGAACATTGTAG	
LXRβ	Forw	GGAGATCGTGGACTTCGCTA	qRT-PCR
	Rev	ACACTCTGTCTCGTGGTTGT	

Human PC specimens

The human PC tissue arrays, including 100 primary PC tumor tissues and 80 paired normal pancreatic tissues, were obtained from Shanghai Outdo Biotech (Shanghai, China). In addition, 24 PC tumor tissues and four paired normal pancreatic tissues were provided by Chang Zhou Hospital. The clinical characteristics of the patients are presented in Extended Table 1. The study was approved by Ethical Committee of Soochow University prior to sample analysis. Tissue samples were collected, after written informed consent, from patients who underwent pancreatic resection for PC.

Preprocessing of RNA-seq data

All second-generation RNA-seq data for PNKP, SREBF1, and LXRα were recorded from Oncomine database (https://www.oncomine.org). Next, the values were calculated and normalized using GraphPad Prism software.

Immunohistochemistry

PNKP protein levels in the tissue samples were detected by immunohistochemistry as described previously [64]. The slides were then stained with 3,3-diaminobenzidine solution and observed and imaged using a Leica microscope.

Cell culture

The human PC cell lines Patu8988 and Panc1were obtained from Cell Bank of the Shanghai Institute of Biochemistry and Cell Biology, Chinese Academy of Sciences (Shanghai, China). Other cells used in our study were from ATCC and Cell Bank of the Shanghai Institute of Biochemistry and Cell Biology, Chinese Academy of Sciences. The cells were mycoplasma free, and cultured in Dulbecco's Modified Eagle Medium (DMEM) (high glucose) supplemented with 10% heat-inactivated fetal bovine serum, 100 U/mL penicillin G, and 100 µg/mL streptomycin under a humidified atmosphere of 5% CO_2 at 37 °C as previously described [65].

Cell UVB radiation

The UVB source was a HL-2000 UV Crosslinker (UVP, Upland, CA, USA), which was used to deliver an energy spectrum of UVB radiation (280–320 nm; peak intensity, 302 nm), and 1 or 2 mJ/cm^2 of UVB was exposed to cells.

Cell growth assay

Cell growth was measured using the Alamarblue assay as we described previously [65]. In short, cells were seeded in 96-well plates for 24 h in DMEM complete medium with either triptonide at the concentrations of 0–8 nM or dimethyl sulphoxide as a control. After 70 h incubation, 10 µL of Alamarblue solution was added to each well. The plates were incubated at 37 °C, 5% CO_2 for 2 h, and the dual fluorescence wavelength absorbance at 560 nm and 590 nm were measured using SpectraMax M5 multi-detection reader. The IC_{50}, which is defined as the drug concentration at which cell growth was inhibited by 50%, was determined using SPSS 16.0 software.

Western blotting

Proteins from pancreatic cells were extracted using the M-PER Mammalian Protein Extraction Kit (Thermo Scientific, Massachusetts, USA) as reported previously [66]. Equal amounts of protein were loaded in each lane and resolved by sodium dodecyl sulphate-polyacrylamide gel electrophoresis with Tris-glycine running buffer. Separated proteins were then transferred to nitrocellulose membranes. Membranes were blocked with 5% nonfat milk and incubated with primary antibodies to PNKP, SREBP1, and LXRα at 4 °C overnight, followed by incubation with HRP-coupled secondary antibody for 1 h at room temperature. Blots were visualized using enhanced chemiluminescence detection reagents and exposed to X-ray film.

Colony formation assay

The tumorigenicity of the tumor cells was measured via a colony-forming assay as previously described [67]. The tumor cells were incubated with triptonide at doses of 0–8 nM for 72 h, harvested, and then enumerated following trypan blue staining. The 35-mm dishes were coated with 0.5% agarose supplemented with complete DMEM medium. After the bottom layer had solidified, 2000 living cells in 1.6 mL of complete medium were mixed with 0.15 mL 4% low-melting agarose and then put in the dishes and allowed to solidify. Then, the dishes were incubated at 37 °C in an atmosphere containing 5% CO_2 for 14 d without further addition of triptonide. The colonies were counted and imaged under a Zoom-stereo microscope SZX16 (OLYMPUS, Tokyo, Japan).

Human PC cell xenograft in mice

All mice used in this study were maintained in a laminar airflow cabinet under specific pathogen-free conditions in a 12-h light–dark cycle. Animal care and experiments followed the approved animal protocols of Soochow University Animal Care and Use Committee. The cancer cell xenograft in mice was performed as described previously [65]. In brief, 6-week-old female nude mice (18–22 g) were randomly divided into two groups (eight mice per group), and then each mouse was subcutaneously injected with pre-cold (4 °C) 300 μL of a mixture of PC cell line Patu8988 (1×10^7 cells in 200 μL) and Matrigel (100 μL).

Prevention of PC cell tumorigenesis in the xenograft mice by triptonide

After xenograft, the mice were intraperitoneally injected daily with either triptonide (5 mg/kg/d) or saline as a control. The body weight of each mouse was recorded, and the tumor volume was monitored using digital calipers every other day. Tumor growth rate was calculated according to the following formula: tumor volume $= 0.55 \times \text{length} \times \text{width}^2$. After treatment with triptonide for 73 days, blood samples were collected from the eye veins of the animals and stored in blood collection tubes containing sodium citrate solution. Then the mice were killed, and the solid tumors were excised, weighed, and imaged. Various important organs, including the hearts, livers, spleens, lungs, and kidneys, were also collected. The blood samples were assessed using Automated Hematology Analyzer KX-21N (Sysmex Corporation, Kobe, Japan). The hearts, livers, spleens, lungs, and kidneys were weighed, and the organ index was calculated according to the following equation: organ index = organ weight (mg)/body weight (g).

Wright–Giemsa staining

PC cells were grown on slides in six-well plates and incubated with triptonide at the concentrations of 0–8 nM for 72 h. After incubation, the cells were rinsed with phospate-buffered saline (PBS) and stained using Wright–Giemsa solution according to the manufacturer's instructions.

Transmission electron microscope analysis

Cells were fixed with 1% (w/v) osmium tetroxide for 2 h at room temperature, and dehydrated with ethanol. Subsequently, the cells were embedded by acetone, and the sections were stained with uranly acetate and lead citrate, and observed under a H600 transmission electron microscope (Hitachi Limited, Tokyo, Japan).

Cell apoptosis assay

The cell apoptosis was assessed using Annexin V and propodium iodide double staining or 7-AAD and phycoerythrin (PE) double staining. In brief, cells were incubated with the indicated doses of triptonide for 3d, 6d, and 9d, respectively, harvested, and then stained with fluorescein isothiocyanate-labeled Annexin V and PI or 7-AAD and PE. Then, the stained cells were analyzed by flow cytometry (Becton Dickinson FACSCalibur, Franklin, Lakes, NJ, USA).

Comet assay

The alkaline comet assay was used to assess intracellular DSBs and performed as described according to the protocols provided by the manufacturer (Trevigen). In short, PC cells were grown on six-well plates, treated with triptonide at the indicated doses for 72 h, lysed with lysis buffer, and subjected to electrophoresis. DNA content was stained with ethidium bromide. The slides were photographed digitally, and the amounts of DNA tails were analyzed using a photography software.

RT-PCR

Total RNA was extracted from cells and treated with RNase-free DNase I. The cDNA was generated by reverse transcription using RevertAid First-Strand cDNA Synthesis Kit (Fermentas Life Sciences, St. Leon-Rot, Germany) and oligo (dT) in a 20 μL reaction containing 5 μg of total RNA. RT-PCR was performed in each 25 μL PCR reaction containing 0.5 μL diluted cDNA, primers, dNTPs, and TaKaRa Taq DNA Polymerase. The PCR reaction contained an initial denaturation at 94 °C for 3 min, followed by 22–35 cycles of denaturation at 94 °C for 30 s, annealing at 68 °C for 30 s, and extension at 72 °C for 1 min. Number of cycles was dependent on the primer length and the molecular

weights of the target genes. PCR products were analyzed by 1% agarose gel.

Quantitative real-time PCR

Quantitative real-time RT-PCR (qRT-PCR) analysis was carried out using Platinum SYBR Green qPCR Super Mix-UDG kits (Life Technologies, Carlsbad, CA, USA) on an ABI Prism 7500 real-time PCR system (Applied Biosystems, Foster City, CA, USA) according to the manufacturer's instructions [66]. Threshold cycle (Ct) values of *PNKP* and *SREBF1* mRNA were equilibrated to β-actin, which was used as an internal control. Relative expression was calculated using the ΔΔCt method as previously described.

Luciferase assay for measurement of gene promoter activity

The genomic DNA fragments in the 5'flanking promoter region of PNKP and SREBF1 genes were cloned into luciferase reporter vector pGL4.17. Patu8988 cells were transfected with the pGL4.17-PNKP or pGL4.17-SREBF1 promoter constructs or control pGL4.17 using Lipofectamine 2000 reagent (Invitrogen) and selected using G418 for 3–4 weeks. The stably transfected cells were treated with triptonide at the doses of 0–8 nM. The luciferase activity in cell lysates was measured using the Dual-Luciferase Reporter assay kit (Promega, Madison, WI, USA).

Recombinant protein expression and purification

The full-length LXRα cDNA was cloned into a pET28a vector with a six-residue His tag at the N-terminus. The pET28a-LXRa plasmid was transformed into *Escherichia coli* BL21 (DE3) cells. Transformed cells in 10 L of LB medium ($OD_{600} = 0.6$) were induced with 0.05 mmol/L isopropyl-β-D-thiogalactopyranoside for 3 h at 16 °C, harvested, and resuspended in 300 mL lysis buffer (25 mmol/L HEPES, pH 8.6; 500 mmol/L NaCl; 10% glycerol; 3 mmol/L β-mercaptoethanol; 1 mmol/L phenylmethylsulfonyl fluoride; 0.5 mmol/L ethylenediaminetetraacetic acid (EDTA); 1 mg/mL lysozyme). The suspension was incubated at 4 °C for 60 min with shaking and then sonicated for 5 min. The cell lysates were centrifuged at 13,000 rpm for 30 min, and the supernatant was applied to a nickel column (Ni-NTA). The column was washed with 40 mL buffer A (25 mmol/L HEPES, pH 7.5; 500 mmol/L NaCl; 100 mmol/L imidazole) and eluted with 10 mL buffer B (25 mmol/L HEPES, pH 7.5; 500 mmol/L NaCl; 500 mmol/L imidazole). The eluted LXRα was concentrated from 2 mL to 1 mg/mL using a spin column with a filter by spinning at 10,000 × *g*, and freshly used in several experiments.

SPR assay

The direct binding of triptonide to LXRα was measured using a fully automated SPR-based Biacore T200 (GE company, Fairfield, CT, USA) according to the manufacturer's instructions. Purified LXRα (0.1 mg/mL) was immobilized on a CM5 sensor chip according to the Biacore manual. Triptonide was serially diluted with HBS buffer (10 mmol/L HEPES, 150 mmol/L NaCl, 3 mmol/L EDTA, 0.05% surfactant P20, 0.1% DMSO). The samples were injected into the channels at a flow rate of 30 μL/min and then washed with HBS buffer. The binding response unit values of triptonide to LXRα were recorded directly by the Biacore T200 instrument and normalized by subtracting the signal from that obtained from vehicle (0.1% DMSO).

Pull-down assay for determining the direct binding of triptonide to LXRα protein

Triptonide was first dissolved in methanol buffer at a concentration of 1 mg/ml and then incubated at final concentration of 10 μg/ml with 0.5 ml recombinant LXRα protein-Ni-NTA beads or control Ni-NTA beads at 4 °C for 60 min (both LXRα protein-Ni-NTA beads and control Ni-NTA beads were pre-blocked by 1% BSA for 1 h at room temperature). The beads were washed five times with wash buffer to remove free triptonide. The LXRα protein-bound triptonide was eluted with elution buffer, and the eluted triptonide was separated by HPLC and analyzed using mass spectrometry.

CD spectroscopic measurements

Purified LXRα (1 mg/mL) was mixed with 100 μM triptonide. CD spectra were recorded on a Jasco J-715 spectropolarimeter (Tokyo, Japan) at 25 ± 0.2 °C with a rectangular quartz cell with a 0.01-cm optical path length (Hellma, Plainview, NY, USA). Temperature control was provided by a Peltier thermostat equipped with magnetic stirring. Each spectrum represents the average of three scans obtained by collecting data at a scan speed of 100 nm/min. CD curves of LXRα-triptonide mixtures were corrected by subtracting spectral contributions of ligand-free LXRα.

Cell transfection

PC Patu8988 and Panc1 cells were transfected with either VENUS-PNKP cDNA, VENUS-LXRα cDNA, or control VENUS vector using Lipofectamine 2000 (Invitrogen) according to the manufacturer's instructions. The GFP-positive transfected cells were sorted by flow cytometry, and the stably transfected cells were expanded. In addition, Patu8988 cells

were transfected with PNKP shRNA-Hu6-MCS-Ubiquitin-EGFP-IRES-puromycin (PNKP shRNA sequence: 5′-AGAGATGACGGACTCCTCT-3′) or SREBF1 shRNA- Hu 6-MCS-Ubiquitin-EGFP-IRES-puromycin (SREBF1 shRNA sequence: 5′-TCTCCATCAGTTCCAGCAT-3′) or LXRα shRNA- Hu6-MCS-Ubiquitin-EGFP-IRES-puromycin (LXRα shRNA sequence: 5′-ctGAAGAAACTGAAGCGGCAA-3′) or control Hu6-MCS-Ubiquitin-EGFP-IRES-puromycin vector. PNKP, SREBF1, and LXRα protein levels in the stably transfected cells were determined by Western blotting.

TUNEL assay

Cell apoptosis was detected using the TUNEL assay kit. In brief, PC cells were seeded on glass cover slips in a six-well plate at 50,000 cells per well and incubated for 12 h, and then treated with triptonide at the concentrations of 0–8 nM for 72 h. The cells were fixed in a 4% paraformaldehyde solution for 20 min, permeabilized with 0.3% Triton X-100 for 10 min, washed for three times with PBS, and stained by the fresh TUNEL assay solution. After incubation in the dark at 37 °C for 60 min, the cells were washed three times with PBS, then incubated with 4.6-diamidino-2-phenylindole for 10 min in the dark. The slides were washed with PBS for three times and sealed with the anti-fluorescence quenching sealant. The apoptotic cells were imaged using OLYMPUS FSX-100 confocal microscopy.

Statistical analysis

The data shown in this study represent the mean ± S.E. of three independent experiments. Differences between the groups were assessed by one-way analysis of variance using GraphPad Prism 7.02 software. The significance of differences was indicated as $*P < 0.05$ and $**P < 0.01$.

Data availability

Available by request from the corresponding author or from commercial sources when applicable.

Acknowledgements This study was supported by grants from the National Natural Science Foundation of China (grants no. 81372376, no. 81572257, no. 81703595, and no. 81772535); Key Laboratory of Stem Cells and Biomedical Materials of Jiangsu Province and the Chinese Ministry of Science and Technology; State Key Laboratory of Radiation Medicine and Protection, School of Radiation Medicine and Protection; a project funded by the Priority Academic Program Development of Jiangsu Higher Education Institutions (PAPD); Jiangsu Province's Key Discipline of Medicine (XK201118); the 2011 Collaborative Innovation Center of Hematology of Jiangsu Province; Natural Science Funds of Jiangsu Colleges and Universities (No. 16KJB310015); and Jiangsu Key Laboratory of Preventive and Translational Medicine for Geriatric Diseases. We thank Dr. Jian Zhou, Bowen Chen, Jiaqi Zheng, and Mingcheng Guan for collecting cancer patient samples and data.

Compliance with ethical standards

Conflict of interest The authors declare that they have no conflict of interest.

Publisher's note Springer Nature remains neutral with regard to jurisdictional claims in published maps and institutional affiliations.

References

1. Khanna A. DNA damage in cancer therapeutics: a boon or a curse. Cancer Res 2015;75:2133–38.
2. Basu AK. DNA damage, mutagenesis and cancer. Int J Mol Sci. 2018;19:pii: E970.
3. Desai A, Yan Y, Gerson SL. Advances in therapeutic targeting of the DNA damage response in cancer. DNA Repair (Amst). 2018;66-67:24–9.
4. Toma M, Skorski T, Sliwinski T. DNA double strand break repair - related synthetic lethality. Curr Med Chem. 2019;26:1446–82.
5. Wright SM, Woo YH, Alley TL, Shirley BJ, Akeson EC, Snow KJ, et al. Complex oncogenic translocations with gene amplification are initiated by specific DNA breaks in lymphocytes. Cancer Res 2009;69:4454–60.
6. Waddell N, Pajic M, Patch AM, Chang DK, Kassahn KS, Bailey P, et al. Whole genomes redefine the mutational landscape of pancreatic cancer. Nature 2015;518:495–501.
7. Bailey P, Chang DK, Nones K, Johns AL, Patch AM, Gingras MC, et al. Genomic analyses identify molecular subtypes of pancreatic cancer. Nature 2016;531:47–52.
8. Liu IH, Ford JM, Kunz PL. DNA-repair defects in pancreatic neuroendocrine tumors and potential clinical applications. Cancer Treat Rev. 2016;44:1–9.
9. Osterman M, Kathawa D, Liu D, Guo H, Zhang C, Li M, et al. Elevated DNA damage response in pancreatic cancer. Histochem Cell Biol. 2014;142:713–20.
10. Miwa S, Yano S, Yamamoto M, Matsumoto Y, Uehara F, Hiroshima Y, et al. Real-time fluorescence imaging of the DNA damage repair response during mitosis. J Cell Biochem. 2015;116:661–66.
11. Cannon MV, van Gilst WH, de Boer RA. Emerging role of liver X receptors in cardiac pathophysiology and heart failure. Basic Res Cardiol. 2016;111:3.
12. Hsieh J, Koseki M, Molusky MM, Yakushiji E, Ichi I, Westerterp M, et al. TTC39B deficiency stabilizes LXR reducing both atherosclerosis and steatohepatitis. Nature 2016;535:303–7.
13. DeBose-Boyd RA, Ou J, Goldstein JL, Brown MS. Expression of sterol regulatory element-binding protein 1c (SREBP-1c) mRNA in rat hepatoma cells requires endogenous LXR ligands. Proc Natl Acad Sci USA. 2001;98:1477–82.
14. Kim K, Kim KH, Kim HH, Cheong J. Hepatitis B virus X protein induces lipogenic transcription factor SREBP1 and fatty acid synthase through the activation of nuclear receptor LXRalpha. Biochem J. 2008;416:219–30.
15. Li C, Yang W, Zhang J, Zheng X, Yao Y, Tu K, et al. SREBP-1 has a prognostic role and contributes to invasion and metastasis in human hepatocellular carcinoma. Int J Mol Sci. 2014;15:7124–38.
16. Sun Y, He W, Luo M, Zhou Y, Chang G, Ren W, et al. SREBP1 regulates tumorigenesis and prognosis of pancreatic cancer through targeting lipid metabolism. Tumour Biol. 2015;36:4133–41.
17. Villa GR, Hulce JJ, Zanca C, Bi J, Ikegami S, Cahill GL, et al. An LXR-cholesterol axis creates a metabolic co-dependency for brain cancers. Cancer Cell 2016;30:683–93.

18. Reynolds JJ, Walker AK, Gilmore EC, Walsh CA, Caldecott KW. Impact of PNKP mutations associated with microcephaly, seizures and developmental delay on enzyme activity and DNA strand break repair. Nucleic Acids Res. 2012;40:6608–19.
19. Nakashima M, Takano K, Osaka H, Aida N, Tsurusaki Y, Miyake N, et al. Causative novel PNKP mutations and concomitant PCDH15 mutations in a patient with microcephaly with early-onset seizures and developmental delay syndrome and hearing loss. J Hum Genet. 2014;59:471–74.
20. Chatterjee A, Saha S, Chakraborty A, Silva-Fernandes A, Mandal SM, Neves-Carvalho A, et al. The role of the mammalian DNA end-processing enzyme polynucleotide kinase 3'-phosphatase in spinocerebellar ataxia type 3 pathogenesis. PLoS Genet. 2015;11: e1004749.
21. Kalasova I, Hanzlikova H, Gupta N, Li Y, Altmuller J, Reynolds JJ, et al. Novel PNKP mutations causing defective DNA strand break repair and PARP1 hyperactivity in MCSZ. Neurol Genet. 2019;5:e320.
22. Gao R, Chakraborty A, Geater C, Pradhan S, Gordon KL, Snowden J, et al. Mutant huntingtin impairs PNKP and ATXN3, disrupting DNA repair and transcription. Elife 2019;8:e42988.
23. Mereniuk TR, El GMA, Mendes-Pereira AM, Lord CJ, Ghosh S, Foley E, et al. Synthetic lethal targeting of PTEN-deficient cancer cells using selective disruption of polynucleotide kinase/phosphatase. Mol Cancer Ther. 2013;12:2135–44.
24. Shire Z, Vakili MR, TDR M, Hall DG, AUID- Oho, Lavasanifar A, et al. Nanoencapsulation of novel inhibitors of PNKP for selective sensitization to ionizing radiation and irinotecan and induction of synthetic lethality. Mol Pharm. 2018;15:2316–26.
25. Chalasani SL, Kawale AS, Akopiants K, Yu Y, Fanta M, Weinfeld M, et al. Persistent 3'-phosphate termini and increased cytotoxicity of radiomimetic DNA double-strand breaks in cells lacking polynucleotide kinase/phosphatase despite presence of an alternative 3'-phosphatase. DNA Repair (Amst). 2018;68:12–24.
26. Smith AL, Alirezaie N, Connor A, Chan-Seng-Yue M, Grant R, Selander I, et al. Candidate DNA repair susceptibility genes identified by exome sequencing in high-risk pancreatic cancer. Cancer Lett. 2016;370:302–12.
27. Khan MA, Azim S, Zubair H, Bhardwaj A, Patel GK, Khushman M, et al. Molecular drivers of pancreatic cancer pathogenesis: looking inward to move forward. Int J Mol Sci. 2017;18:779–803.
28. Yoshikawa T, Shimano H, Yahagi N, Ide T, Amemiya-Kudo M, Matsuzaka T, et al. Polyunsaturated fatty acids suppress sterol regulatory element-binding protein 1c promoter activity by inhibition of liver X receptor (LXR) binding to LXR response elements. J Biol Chem. 2002;277:1705–11.
29. Kamisuki S, Shirakawa T, Kugimiya A, Abu-Elheiga L, Choo HY, Yamada K, et al. Synthesis and evaluation of diarylthiazole derivatives that inhibit activation of sterol regulatory element-binding proteins. J Med Chem. 2011;54:4923–27.
30. Chinison J, Aguilar JS, Avalos A, Huang Y, Wang Z, Cameron DJ, et al. Triptonide effectively inhibits wnt/beta-catenin signaling via c-terminal transactivation domain of beta-catenin. Sci Rep. 2016;6:32779.
31. Pan Y, Meng M, Zheng N, Cao Z, Yang P, Xi X, et al. Targeting of multiple senescence-promoting genes and signaling pathways by triptonide induces complete senescence of acute myeloid leukemia cells. Biochem Pharmacol. 2017;126:34–50.
32. Yang P, Dong F, Zhou Q. Triptonide acts as a novel potent anti-lymphoma agent with low toxicity mainly through inhibition of proto-oncogene Lyn transcription and suppression of Lyn signal pathway. Toxicol Lett 2017;278:9–17.
33. Han H, Du L, Cao Z, Zhang B, Zhou Q. Triptonide potently suppresses pancreatic cancer cell-mediated vasculogenic mimicry by inhibiting expression of VE-cadherin and chemokine ligand 2 genes. Eur J Pharm. 2018;818:593–603.
34. Zhang B, Meng M, Xiang S, Cao Z, Xu X, Zhao Z, et al. Selective activation of tumor-suppressive MAPKP signaling pathway by triptonide effectively inhibits pancreatic cancer cell tumorigenicity and tumor growth. Biochem Pharmacol 2019;166:70–81.
35. Fukuchi J, Kokontis JM, Hiipakka RA, Chuu CP, Liao S. Antiproliferative effect of liver X receptor agonists on LNCaP human prostate cancer cells. Cancer Res 2004;64:7686–89.
36. Lo SG, Bovenga F, Murzilli S, Salvatore L, Di TG, Martelli N, et al. Liver X receptors inhibit proliferation of human colorectal cancer cells and growth of intestinal tumors in mice. Gastroenterology 2013;144:1497–507.
37. Pommier AJ, Dufour J, Alves G, Viennois E, De Boussac H, Trousson A, et al. Liver x receptors protect from development of prostatic intra-epithelial neoplasia in mice. PLoS Genet 2013;9: e1003483.
38. Derangere V, Chevriaux A, Courtaut F, Bruchard M, Berger H, Chalmin F, et al. Liver X receptor beta activation induces pyroptosis of human and murine colon cancer cells. Cell Death Differ. 2014;21:1914–24.
39. Sharma B, Gupta V, Dahiya D, Kumar H, Vaiphei K, Agnihotri N. Clinical relevance of cholesterol homeostasis genes in colorectal cancer. Biochim Biophys Acta Mol Cell Biol Lipids. 2019;1864:1314–27.
40. Kim S, Lee M, Dhanasekaran DN, Song YS. Activation of LXRa/beta by cholesterol in malignant ascites promotes chemoresistance in ovarian cancer. BMC Cancer 2018;18:1232.
41. Wang K, Xu T, Ruan H, Xiao H, Liu J, Song Z, et al. LXRalpha promotes cell metastasis by regulating the NLRP3 inflammasome in renal cell carcinoma. Cell Death Dis. 2019;10:159.
42. Baek AE, Yu YA, He S, Wardell SE, Chang CY, Kwon S, et al. The cholesterol metabolite 27 hydroxycholesterol facilitates breast cancer metastasis through its actions on immune cells. Nat Commun 2017;8:864.
43. Shen Z, Zhu D, Liu J, Chen J, Liu Y, Hu C, et al. 27-Hydroxycholesterol induces invasion and migration of breast cancer cells by increasing MMP9 and generating EMT through activation of STAT-3. Environ Toxicol Pharm. 2017;51:1–8.
44. Marwarha G, Raza S, Hammer K, Ghribi O. 27-hydroxycholesterol: a novel player in molecular carcinogenesis of breast and prostate cancer. Chem Phys Lipids. 2017;207:108–26.
45. Zhang L, Liu M, Liu J, Li X, Yang M, Su B, et al. 27-Hydroxycholesterol enhanced osteoclastogenesis in lung adenocarcinoma microenvironment. J Cell Physiol. 2019;234:12692–700.
46. Zhao Y, Li H, Zhang Y, Li L, Fang R, Li Y, et al. Oncoprotein HBXIP modulates abnormal lipid metabolism and growth of breast cancer cells by activating the LXRs/SREBP-1c/FAS signaling cascade. Cancer Res 2016;76:4696–707.
47. Ji L, Zhang B, Zhao G. Liver X receptor alpha (LXRalpha) promoted invasion and EMT of gastric cancer cells by regulation of NF-kappaB activity. Hum Cell 2017;30:124–32.
48. Kim MJ, Choi MY, Lee DH, Roh GS, Kim HJ, Kang SS, et al. O-linked N-acetylglucosamine transferase enhances secretory clusterin expression via liver X receptors and sterol response element binding protein regulation in cervical cancer. Oncotarget 2018;9:4625–36.
49. Collins JL, Fivush AM, Watson MA, Galardi CM, Lewis MC, Moore LB, et al. Identification of a nonsteroidal liver X receptor agonist through parallel array synthesis of tertiary amines. J Med Chem. 2002;45:1963–66.
50. Houck KA, Borchert KM, Hepler CD, Thomas JS, Bramlett KS, Michael LF, et al. T0901317 is a dual LXR/FXR agonist. Mol Genet Metab. 2004;83:184–87.
51. Hu Y, Zang J, Cao H, Wu Y, Yan D, Qin X, et al. Liver X receptors agonist GW3965 re-sensitizes gefitinib-resistant human non-small cell lung cancer cell to gefitinib treatment by inhibiting NF-kappaB in vitro. Oncotarget. 2017;8:15802–14.

52. Ju X, Huang P, Chen M, Wang Q. Liver X receptors as potential targets for cancer therapeutics. Oncol Lett. 2017;14:7676–80.
53. Hiramitsu S, Ishikawa T, Lee WR, Khan T, Crumbley C, Khwaja N, et al. Estrogen receptor beta-mediated modulation of lung cancer cell proliferation by 27-hydroxycholesterol. Front Endocrinol (Lausanne). 2018;9:470.
54. Gibson DA, Collins F, Cousins FL, Esnal ZA, PTK S. The impact of 27-hydroxycholesterol on endometrial cancer proliferation. Endocr Relat Cancer. 2018;25:381–91.
55. Tian W, Pang W, Ge Y, He X, Wang D, Li X, et al. Hepatocyte-generated 27-hydroxycholesterol promotes the growth of melanoma by activation of estrogen receptor alpha. J Cell Biochem. 2018;119:2929–38.
56. Codini M, Cataldi S, Lazzarini A, Tasegian A, Ceccarini MR, Floridi A, et al. Why high cholesterol levels help hematological malignancies: role of nuclear lipid microdomains. Lipids Health Dis. 2016;15:4.
57. Jubinville E, Routhier J, Maranda-Robitaille M, Pineault M, Milad N, Talbot M, et al. Pharmacological activation of liver X receptor during cigarette smoke exposure adversely affects alveolar macrophages and pulmonary surfactant homeostasis. Am J Physiol Lung Cell Mol Physiol. 2019;316:L669–78.
58. Nelson ER, Wardell SE, Jasper JS, Park S, Suchindran S, Howe MK, et al. 27-Hydroxycholesterol links hypercholesterolemia and breast cancer pathophysiology. Science 2013;342:1094–98.
59. Porcelli L, Quatrale AE, Mantuano P, Leo MG, Silvestris N, Rolland JF, et al. Optimize radiochemotherapy in pancreatic cancer: PARP inhibitors a new therapeutic opportunity. Mol Oncol. 2013;7:308–22.
60. Karnak D, Engelke CG, Parsels LA, Kausar T, Wei D, Robertson JR, et al. Combined inhibition of Wee1 and PARP1/2 for radiosensitization in pancreatic cancer. Clin Cancer Res. 2014;20:5085–96.
61. Jin WH, Hoffe SE, Shridhar R, Strom T, Venkat P, Springett GM, et al. Adjuvant radiation provides survival benefit for resected pancreatic adenocarcinomas of the tail. J Gastrointest Oncol. 2018;9:487–94.
62. Srivastava P, Sarma A, Chaturvedi CM. Targeting DNA repair with PNKP inhibition sensitizes radioresistant prostate cancer cells to high LET radiation. PLoS ONE 2018;13:e0190516.
63. Zins M, Matos C, Cassinotto C. Pancreatic adenocarcinoma staging in the era of preoperative chemotherapy and radiation therapy. Radiology 2018;287:374–90.
64. Liu W, Meng M, Zhang B, Du L, Pan Y, Yang P, et al. Dehydroeffusol effectively inhibits human gastric cancer cell-mediated vasculogenic mimicry with low toxicity. Toxicol Appl Pharm. 2015;287:98–110.
65. Zhang B, Han H, Fu S, Yang P, Gu Z, Zhou Q, et al. Dehydroeffusol inhibits gastric cancer cell growth and tumorigenicity by selectively inducing tumor-suppressive endoplasmic reticulum stress and a moderate apoptosis. Biochem Pharmacol. 2016;104:8–18.
66. Liu W, Lv C, Zhang B, Zhou Q, Cao Z. MicroRNA-27b functions as a new inhibitor of ovarian cancer-mediated vasculogenic mimicry through suppression of VE-cadherin expression. RNA 2017;23:1019–27.
67. Yang P, Fu S, Cao Z, Liao H, Huo Z, Pan Y, et al. Oroxin B selectively induces tumor-suppressive ER stress and concurrently inhibits tumor-adaptive ER stress in B-lymphoma cells for effective anti-lymphoma therapy. Toxicol Appl Pharm. 2015;288:269–79.

Affiliations

Bo Yang[1,2] · Bin Zhang[3,4,5,6,7,8] · Zhifei Cao[3,4,5,6,9] · Xingdong Xu[10,11] · Zihe Huo[3,4,5,6] · Pan Zhang[3,4,5,6] · Shufen Xiang[3,4,5,6] · Zhe Zhao[3,4,5,6] · Chunping Lv[3,4,5,6] · Mei Meng[3,4,5,6] · Gaochuan Zhang[12] · Liang Dong[13] · Shucheng Shi[1,2] · Lan Yang[1,2] · Quansheng Zhou[3,4,5,6]

[1] Department of General Surgery, The Third Affiliated Hospital of Soochow University, Suzhou, Jiangsu 215123, P. R. China

[2] The First People's Hospital of Changzhou, Changzhou 213003, P. R. China

[3] Cyrus Tang Hematology Center, Jiangsu Institute of Hematology, Soochow University, Suzhou, Jiangsu 215123, P. R. China

[4] State Key Laboratory of Radiation Medicine, Soochow University, Suzhou, Jiangsu 215123, P. R. China

[5] Key Laboratory of Thrombosis and Hemostasis, Ministry of Health, Soochow University, Suzhou, Jiangsu 215123, P. R. China

[6] 2011 Collaborative Innovation Center of Hematology, Soochow University, Suzhou, Jiangsu 215123, P. R. China

[7] Center of Systems Medicine, Institute of Basic Medical Sciences, Chinese Academy of Medical Sciences & Peking Union Medical College, Beijing 100005, China

[8] Suzhou Institute of Systems Medicine, Suzhou 215123, China

[9] Department of Pathology, The Second Affiliated Hospital of Soochow University, Suzhou, Jiangsu 215123, P. R. China

[10] Department of General Surgery, The People's Hospital of China, Three Gorges University, Yichang 443000, P. R. China

[11] The First People's Hospital of Yichang, Yichang 443000, P. R. China

[12] Department of Bioinformatics, College of Basic Medical Science, Soochow University, Suzhou, Jiangsu 215123, P. R. China

[13] Department of Pathology, College of Basic Medical Science, Soochow University, Suzhou, Jiangsu 215123, P. R. China